

Oscillator strengths in the framework of equation of motion multilevel CC3

Alexander C. Paul,[†] Sarai D. Folkestad,[†] Rolf H. Myhre,[†] and Henrik Koch^{*,†,‡}

[†]*Department of Chemistry, Norwegian University of Science and Technology, NTNU, 7491
Trondheim, Norway*

[‡]*Scuola Normale Superiore, Piazza dei Cavalieri 7, 56126 Pisa, Italy*

E-mail: henrik.koch@sns.it

Abstract

We present an efficient implementation of the equation of motion oscillator strengths for the closed-shell multilevel coupled cluster singles and doubles with perturbative triples method (MLCC3) in the electronic structure program e^T . The orbital space is split into an active part treated with CC3 and an inactive part computed at the coupled cluster singles and doubles (CCSD) level of theory. Asymptotically, the CC3 contribution scales as $\mathcal{O}(n_v n_v^3 n_o^3)$ floating-point operations (FLOP), where n_v is the total number of virtual orbitals while n_v and n_o are the number of active virtual and occupied orbitals, respectively. The CC3 contribution, thus, only scales linearly with the full system size and can become negligible compared to the cost of CCSD. We demonstrate the capabilities of our implementation by calculating the UV-VIS spectrum of azobenzene and a core excited state of betaine 30 with more than 1000 molecular orbitals.

Introduction

Coupled cluster theory is one of the most accurate models when spectroscopic properties of small and medium sized molecules are investigated.¹⁻³ Due to its high accuracy and relatively feasible computational scaling as $\mathcal{O}(n_V^4 n_O^2)$, CCSD is the most widely used variant of coupled cluster. Despite its accuracy for valence excited states, larger errors occur when considering core excited states or double excitation dominated states.⁴⁻⁹ Including triple excitations in the parametrization of the wave function improves the description of such states. However, the computational cost and the memory requirement increase to $\mathcal{O}(n_V^5 n_O^3)$ and $\mathcal{O}(n_V^3 n_O^3)$, respectively for CCSDT.^{10,11} Approximating triples amplitudes with perturbation theory can reduce the computational cost to $\mathcal{O}(n_V^4 n_O^3)$ and the required memory to $\mathcal{O}(n_V^2 n_O^2)$.

Triples corrections can be classified as iterative and noniterative models. In noniterative models, corrections to the CCSD excitation energy are obtained by expanding the excitation energy using many-body perturbation theory (MBPT). The advantage of a noniterative approach is that the triples correction is only computed once. The disadvantage, however, is that transition moments cannot be easily defined.^{9,12} The noniterative models include CCSDR(1a), CCSDR(1b) and CCSDR(3) which are derived from the iterative methods CCSDT-1a, CCSDT-1b and CC3, respectively.^{9,13-16} Other noteworthy examples are CREOM-CCSD(T), EOMIP-CCSD* —developed specifically for ionized states— and EOM-CCSD(T)(a)* which introduces corrections to both the CCSD ground and the excited states.¹⁷⁻²⁰

The best-known methods for including triples excitations iteratively are CC3 and CCSDT-n.^{13,14} Both CCSDT-1 and CC3 scale asymptotically as $\mathcal{O}(n_V^4 n_O^3)$, but CC3 includes single excitations to infinite order leading to an improved description of ground and excited states.¹⁴ The advantage of iterative models is that they are more robust²¹ and provide a consistent definition of other properties than the energy.²² However, that comes at the cost of iteratively converging equations scaling as $\mathcal{O}(n_V^4 n_O^3)$. Nevertheless, with current implementations systems of around 400 basis functions can be routinely treated at the CC3 level.¹⁶

Due to the success of coupled cluster theory, schemes have been developed to reduce the scaling while keeping the accuracy. Pulay and Sæbø advocated the use of localized molecular orbitals (LMOs), for a compact description of electronic correlation in Møller-Plesset (MP) perturbation theory and configuration interaction singles and doubles (CISD).²³⁻²⁷ They used Boys localization for the occupied molecular orbitals and projected atomic orbitals (PAOs) for the virtual space, and reduced the scaling by neglecting the correlation between distant pairs of localized orbitals.²⁴ Werner and Schütz then extended this model to coupled cluster theory with and without a noniterative triples correction.²⁸⁻³⁰ Domain based local pair-natural orbital coupled cluster (DLPNO-CC) methods are also related to this approach.^{31,32} The DLPNO-CC approach has recently been extended to CCSD(T) and also CC3 which was used to calculate the first electronic excited state of a system with more than 1300 basis functions.^{33,34} Reducing the size of the active space based on a distance criterium is certainly successful for ground state properties. For the description of excitation energies and other excited state properties, however, distance measures do not work as well as more diffuse orbitals become more important.³⁵⁻⁴¹ Therefore, larger active spaces have to be employed in these calculations and different orbital spaces are used for the ground and excited states.^{35,36}

Multilevel and embedding methods treat different regions of a system with different levels of theory. The idea of obtaining an accurate description of a large molecular system by coupling the contributions of its subsystems is exploited in QM/MM approaches,⁴²⁻⁴⁷ frozen density embedding,^{48,49} subsystem DFT,^{50,51} and the ONIOM, IMOMO and LMOMO methods.⁵²⁻⁵⁴ Another method related to multilevel coupled cluster (MLCC) was developed by Oliphant and Adamowicz using CCSD for multireference systems by including selected triple and quadruple substitutions.⁵⁵⁻⁵⁷ This scheme was adapted by Köhn and Olsen to include higher order substitutions at reduced cost.^{58,59}

In multilevel coupled cluster (MLCC) one CC wave function is used for the full system but different parts of the system are described with different level of truncation.^{60,61} Considerable savings are achieved by applying the higher order excitation operators in a smaller (active)

subset of the orbitals.⁶² The active orbital space can be selected using localized orbitals — such as Cholesky orbitals⁶³ and projected atomic orbitals (PAOs)²⁴ — or state-selective approaches — such as the correlated natural transition orbitals (CNTOs).⁶⁴ As MLCC is designed for intensive properties, excitation energies or oscillator strengths are accurately reproduced if an appropriate active space is chosen.^{62,64–66} While state-selective approaches are preferred to keep the active space as compact as possible, they are less suited for transition properties especially between excited states, as a consistent active space is needed for all excited states.³⁴ Localized orbitals are only suitable in the cases where the target property is localized in a smaller region of the molecule.

In this paper we report the extension of the MLCC3 method to compute oscillator strengths with CC3 quality but at significantly reduced cost. Employing core-valence separation (CVS), oscillator strengths are also available for core excited states.^{67–69} This allows us to tackle excited states and oscillator strengths of systems with more than 1000 basis functions.

Theory

In this section, we will introduce the closed shell MLCC3 model within the equation of motion (EOM) formalism. For a more detailed derivation we refer to Refs 14,16. Consider the general cluster operator

$$T = \sum_{\mu} \tau_{\mu} X_{\mu}, \tag{1}$$

where X_{μ} is an excitation operator that converts the reference determinant, $|\phi_0\rangle$, into the excited determinant, $|\mu\rangle$, and τ_{μ} is the corresponding amplitude. In MLCC3 with two levels, namely CCSD and CC3, the cluster operator assumes the form

$$T = T_1 + T_2 + T_3^a \tag{2}$$

with

$$\begin{aligned}
T_1 &= \sum_I^A \tau_I^A E_{AI} \\
T_2 &= \frac{1}{2} \sum_{IJ}^{AB} \tau_{IJ}^{AB} E_{AI} E_{BJ} \\
T_3^a &= \frac{1}{6} \sum_{ijk}^{abc} \tau_{ijk}^{abc} E_{ai} E_{bj} E_{ck}
\end{aligned} \tag{3}$$

where E_{AI} and E_{ai} are singlet excitation operators. While the operators T_1 and T_2 excite on the full orbital space indicated by capitalized indices, the triples cluster operator T_3^a only excites in the active orbital space denoted by lower case indices. We use the standard notation where the indices $i, j, k \dots$ refer to occupied, $a, b, c \dots$ to virtual, and $p, q, r \dots$ to general active orbitals. The CC wave function is defined as

$$|\text{CC}\rangle = \exp(T) |\phi_0\rangle \tag{4}$$

and we introduce the similarity transformed Hamiltonian

$$\bar{H} = \exp(-T) \hat{H} \exp(T) \tag{5}$$

where

$$\hat{H} = \sum_{pq} h_{pq} E_{pq} + \frac{1}{2} \sum_{pqrs} (pq|rs) (E_{pq} E_{rs} - E_{ps} \delta_{qr}) + h_{nuc} \tag{6}$$

is the electronic Hamiltonian. To obtain the cluster amplitudes a set of biorthogonal determinants

$$\{ \langle \mu | \} = \{ \langle \mu_1 | \} \oplus \{ \langle \mu_2 | \} \oplus \{ \langle \mu_3^a | \} \tag{7}$$

is defined, where the triply excited determinants, μ_3^a , are restricted to the active space. These determinants are generated using the contravariant excitation operator, \tilde{X}_μ , such that,

$$\langle \mu | \nu \rangle = \langle \phi_0 | \tilde{X}_\mu X_\nu | \phi_0 \rangle = \delta_{\mu\nu}. \quad (8)$$

The coupled cluster energy, E_{CC} , and the cluster amplitudes are then obtained by projection onto the reference determinant and the set of excited determinants, respectively,¹¹

$$E_{CC} = \langle \phi_0 | \bar{H} | \phi_0 \rangle \quad (9)$$

$$\Omega_\mu = \langle \mu | \bar{H} | \phi_0 \rangle = 0. \quad (10)$$

To obtain compact equations we incorporate the effect of the singles cluster operator into the Hamiltonian and obtain the so-called T_1 -transformed Hamiltonian,

$$H = \exp(-T_1) \hat{H} \exp(T_1). \quad (11)$$

In analogy to MBPT, the T_1 -transformed Hamiltonian is split into an effective one-particle operator and a fluctuation potential.

$$H = F + U \quad (12)$$

In CC3 the double excitation amplitudes and the fluctuation potential are treated as first order in the perturbation while the triples amplitudes are considered second order. The single excitation amplitudes are included as zeroth order parameters, as they have a special role as relaxation parameters.^{14,15} Inserting eq (3) and eq (7) into eq (8) and neglecting all terms of third and higher order in the perturbation, we obtain the MLCC3 ground state

equations,

$$\Omega_{\mu_1} = \langle \mu_1 | H + [H, T_2] + [H, T_3^a] | \phi_0 \rangle \quad (13)$$

$$\Omega_{\mu_2} = \langle \mu_2 | H + [H, T_2] + [[H, T_2], T_2] + [H, T_3^a] | \phi_0 \rangle \quad (14)$$

$$\Omega_{\mu_3^a} = \langle \mu_3^a | [H, T_2] + [F, T_3^a] | \phi_0 \rangle. \quad (15)$$

The Fock matrix is not necessarily diagonal in the local orbital basis, but it can be block-diagonalized within the active orbital space, such that the off-diagonal elements do not contribute to the triples amplitudes. Therefore, the triples amplitudes can be expressed in terms of the doubles amplitudes

$$\tau_{ijk}^{abc} = -\frac{1}{\varepsilon_{ijk}^{abc}} \langle \mu_3^a | [H, T_2] | \phi_0 \rangle, \quad (16)$$

where ε_{ijk}^{abc} are the orbital energy differences

$$\varepsilon_{ijk}^{abc} = \varepsilon_a + \varepsilon_b + \varepsilon_c - \varepsilon_i - \varepsilon_j - \varepsilon_k. \quad (17)$$

In equation of motion coupled cluster (EOM-CC) start out from the matrix representation of the similarity transformed Hamiltonian,

$$\bar{\mathbf{H}} = \begin{pmatrix} \langle \phi_0 | \bar{H} | \phi_0 \rangle & \langle \phi_0 | \bar{H} | \nu \rangle \\ \langle \mu | \bar{H} | \phi_0 \rangle & \langle \mu | \bar{H} | \nu \rangle \end{pmatrix}. \quad (18)$$

If the CC ground state equations, eq (8), are converged, the similarity transformed Hamiltonian can be written as,

$$\bar{\mathbf{H}} = \begin{pmatrix} 0 & \boldsymbol{\eta}^T \\ \mathbf{0} & \mathbf{J} \end{pmatrix} + E_{\text{CC}} \mathbf{I}, \quad (19)$$

where $\eta_\nu = \langle \phi_0 | [\bar{H}, X_\nu] | \phi_0 \rangle$ and \mathbf{J} is the so-called Jacobian with matrix elements $\langle \mu | [\bar{H}, X_\nu] | \phi_0 \rangle$.

The eigenvectors of \bar{H} are the EOM states and the corresponding eigenvalues the energies of these states. As the similarity transformed Hamiltonian is non-symmetric, the left and right eigenvectors are not hermitian conjugates, but they are biorthonormal.¹¹

$$\bar{H}\bar{\mathbf{R}}_m = E_m\bar{\mathbf{R}}_m \quad \bar{\mathbf{L}}_m^T\bar{H} = E_m\bar{\mathbf{L}}_m^T \quad \bar{\mathbf{L}}_m^T\bar{\mathbf{R}}_n = \delta_{mn} \quad (20)$$

From the biorthogonality of the EOM states and the structure of the Hamiltonian matrix, we obtain the left and the right ground state,

$$\bar{\mathbf{L}}_0 = \begin{pmatrix} 1 \\ \boldsymbol{\lambda} \end{pmatrix} \quad \bar{\mathbf{R}}_0 = \begin{pmatrix} 1 \\ \mathbf{0} \end{pmatrix}, \quad (21)$$

and the left and right excited states,¹⁶

$$\bar{\mathbf{L}}_m = \begin{pmatrix} 0 \\ \mathbf{L}_m \end{pmatrix} \quad \bar{\mathbf{R}}_m = \begin{pmatrix} -\boldsymbol{\lambda}\mathbf{R}_m \\ \mathbf{R}_m \end{pmatrix}. \quad (22)$$

The parameters $\boldsymbol{\lambda}$ are determined from

$$\boldsymbol{\lambda}^T \mathbf{J} = -\boldsymbol{\eta}, \quad (23)$$

while the parameters of the excited states are determined as eigenvectors of the Jacobian, \mathbf{J} . The MLCC3 Jacobian is given by⁶²

$$\mathbf{J}^{MLCC3} = \begin{pmatrix} \langle \mu_1 | [H + [H, T_2], X_{\nu_1}] | \phi_0 \rangle & \langle \mu_1 | [H, X_{\nu_2}] | \phi_0 \rangle & \langle \mu_1 | [H, X_{\nu_3^a}] | \phi_0 \rangle \\ \langle \mu_2 | [H + [H, T_2 + T_3^a], X_{\nu_1}] | \phi_0 \rangle & \langle \mu_2 | [H + [H, T_2], X_{\nu_2}] | \phi_0 \rangle & \langle \mu_2 | [H, X_{\nu_3^a}] | \phi_0 \rangle \\ \langle \mu_3^a | [H + [H, T_2], X_{\nu_1}] | \phi_0 \rangle & \langle \mu_3^a | [H, X_{\nu_2}] | \phi_0 \rangle & \langle \mu_3^a | [F, X_{\nu_3^a}] | \phi_0 \rangle \end{pmatrix}. \quad (24)$$

The vectors in eq (21) and eq (22) correspond to operators which generate the EOM states

from the Hartree-Fock determinant.

$$\langle \tilde{C}C | = \langle \phi_0 | \left(1 + \sum_{\mu} \lambda_{\mu} \tilde{X}_{\mu} \right) \exp(-T) \quad (25)$$

$$|CC\rangle = \exp(T) |\phi_0\rangle \quad (26)$$

$$\langle m | = \langle \phi_0 | \sum_{\mu} L_{\mu} \tilde{X}_{\mu} \exp(-T) \quad (27)$$

$$|m\rangle = \left(\sum_{\mu} R_{\mu} X_{\mu} - \sum_{\mu} R_{\mu} \lambda_{\mu} \right) \exp(T) |\phi_0\rangle \quad (28)$$

Once the ground and excited states are determined, left and right transition moments can be obtained in terms of left (D^{m-0}) and right (\tilde{D}^{0-m}) transition densities.⁷⁰⁻⁷²

$$\langle \tilde{C}C | A | m \rangle = \sum_{pq} \tilde{D}_{pq}^{0-m} A_{pq} \quad (29)$$

$$\langle m | A | CC \rangle = \sum_{pq} D_{pq}^{m-0} A_{pq} \quad (30)$$

Here, A is a general one-electron operator $A = \sum_{pq} A_{pq} E_{pq}$.

To obtain accurate excitation energies and transition dipole moments, the selection of the active orbital space is crucial. In this paper two approaches are chosen to partition the orbital space. For the cheaper strategy Cholesky orbitals are used for the occupied space. To obtain these orbitals the Hartree-Fock density is Cholesky decomposed using the AOs of the active atoms as pivoting elements.^{63,73}

$$D_{\alpha\beta} = \sum_J C_{\alpha J}^a C_{\beta J}^a + \Delta D_{\alpha\beta} \quad (31)$$

The decomposition is stopped when the size of all active diagonal elements is below a given threshold and the coefficients are simply the elements of the Cholesky vectors $C_{\alpha J}$. The inactive orbitals are then obtained by decomposing the remaining part of the density, ΔD . Projected atomic orbitals have been shown to give a good description of the virtual space

for solvated systems, but also adenosine.^{66,74,75}

The construction of correlated natural transition orbitals is more costly as they are obtained from excitation vectors of a coupled cluster calculation. In MLCC3 we use CNTOs constructed from CCSD excited states to get a compact description of the excited states. The CNTOs are generated by diagonalizing two matrices, denoted by \mathbf{M} and \mathbf{N} , defined as

$$M_{ij} = \sum_a R_i^a R_j^a + \frac{1}{2} \sum_{\substack{ab \\ k}} (1 + \delta_{ai,bk} \delta_{ij}) R_{ik}^{ab} R_{jk}^{ab} \quad (32)$$

$$N_{ab} = \sum_i R_i^a R_i^b + \frac{1}{2} \sum_{\substack{c \\ ij}} (1 + \delta_{ai,cj} \delta_{ab}) R_{ij}^{ac} R_{ij}^{bc}. \quad (33)$$

The eigenvectors of \mathbf{M} and \mathbf{N} correspond to the CNTO transformation matrices for the occupied and virtual CNTOs, respectively. The CNTOs whose eigenvalues sum up to a certain cutoff are chosen as active space

$$1 - \xi_M < \sum_o \lambda_o^M \quad (34)$$

$$1 - \xi_N < \sum_v \lambda_v^N \quad (35)$$

where λ_o^M and λ_v^N are the eigenvalues of \mathbf{M} and \mathbf{N} . To obtain the most compact basis, separate CNTO bases for each excited state would be preferable. However, due to the non-orthogonality of the orbitals, subsequent calculation of transition moments between excited states would be complicated. Therefore, we choose a state averaged approach,

$$\mathbf{M} = \frac{1}{n_{ES}} \sum_i^{n_{ES}} \mathbf{M}_i, \quad \mathbf{N} = \frac{1}{n_{ES}} \sum_i^{n_{ES}} \mathbf{N}_i, \quad (36)$$

where \mathbf{M}_i and \mathbf{N}_i are constructed according to eq (32) and (33) for the i -th excited state and n_{ES} is the number of excited states included in the matrices.

Implementation

The closed shell MLCC3 ground and excited states as well as EOM transition properties have been implemented in the e^T program package.⁷⁶ One of the advantages of MLCC3 compared to other reduced cost methods is that only the space, in which the triples amplitudes are defined, is restricted. Therefore, we can split the occupied and virtual orbitals into active and inactive subsets, and use almost identical code for MLCC3 as for full CC3. The algorithms employed to calculate closed shell CC3 properties in e^T have been detailed in Ref. 16 and only a short summary will be given in this paper. The ground state residual, Ω , and the transformations of a trial vector with the Jacobian are computed in a restricted loop over the occupied indices $i \geq j \geq k$. An n_v^3 -block of triples amplitudes is constructed for a given set of indices $\{i, j, k\}$. Using this structure, the permutational symmetry of the triples amplitudes can be exploited, while utilizing efficient matrix multiplication routines for the contractions of the block of virtual orbitals.⁷⁷⁻⁷⁹ By reformulating the equations in terms of contravariant triples amplitudes

$$\tilde{\tau}_{ijk}^{abc} = 4\tau_{ijk}^{abc} - 2\tau_{jik}^{bac} - 2\tau_{kji}^{cba} - 2\tau_{ikj}^{acb} + \tau_{kij}^{cab} + \tau_{jki}^{bca}, \quad (37)$$

and residuals, $\tilde{\Omega}$, the number of memory-bound reordering operations is reduced. After all contributions to the contravariant residual are collected it is converted back to the covariant form, using the relations

$$\tilde{\Omega}_I^A = \Omega_I^A \quad (38)$$

$$\tilde{\Omega}_{IJ}^{AB} = 2\Omega_{IJ}^{AB} - \Omega_{IJ}^{BA}, \quad \Omega_{IJ}^{AB} = \frac{1}{3}(2\tilde{\Omega}_{IJ}^{AB} + \tilde{\Omega}_{IJ}^{BA}). \quad (39)$$

As in CC3, the τ_3 amplitudes are defined in terms of the τ_2 amplitudes

$$\tau_{ijk}^{abc} = -(\varepsilon_{ijk}^{abc})^{-1} P_{ijk}^{abc} \left(\sum_D \tau_{ij}^{aD} g_{bDck} - \sum_L \tau_{iL}^{ab} g_{Ljck} \right). \quad (40)$$

However, because the triples determinants are restricted to the active space only the summation indices in the expression for τ_3 are over the full space. Here, P_{ijk}^{abc} is a permutation operator creating a sum of all unique permutations of the index pairs ai, bj, ck , and g_{pqrs} are two-electron integrals in the T_1 -transformed basis.¹¹ From eq (40) it is evident that the most memory efficient implementation will make use of two separate arrays for τ_{iL}^{ab} and τ_{ij}^{aD} . Similarly, two vectors are needed for the doubles part of the ground state residual because one index originates from a T_1 -transformed two-electron integral, g_{pqrs} ,

$$\tilde{\Omega}_{iL}^{ab} = \sum_{\substack{c \\ jk}} \tilde{\tau}_{ijk}^{abc} g_{jLkc} \quad (41)$$

$$\tilde{\Omega}_{ij}^{aD} = \sum_{\substack{bc \\ j}} \tilde{\tau}_{ijk}^{abc} g_{Dbkc}, \quad (42)$$

Therefore, the memory requirement and the computational cost of the triples contributions scale linearly with the full size of the system, and the overall asymptotic scaling for constructing the ground state residual is $4n_{\check{v}}n_{\check{v}}^3n_0^3$ floating point operations (FLOP).

The triples amplitudes of the right excitation vector can be expressed as

$$R_{ijk}^{abc} = -\frac{1}{\varepsilon_{ijk}^{abc} - \omega} P_{ijk}^{abc} \left(\sum_D \bar{R}_{ij}^{aD} g_{bDck} - \sum_L \bar{R}_{iL}^{ab} g_{Ljck} + \sum_D \tau_{ij}^{aD} \Upsilon_{bDck} - \sum_L \tau_{iL}^{ab} \Upsilon_{Ljck} \right) \quad (43)$$

where Υ_{bDck} and Υ_{Ljck} are treated as one-index transformed integrals

$$\Upsilon_{bDck} = \sum_E R_k^E g_{bDcE} - \sum_M (R_M^b g_{MDck} + R_m^c g_{bDMk}) \quad (44)$$

$$\Upsilon_{Ljck} = \sum_E (R_j^E g_{LEck} + R_k^E g_{Ljce}) - \sum_M R_M^c g_{LjMk}. \quad (45)$$

and $\bar{R}_{ij}^{ab} = (1 + \delta_{ai,bj})R_{ij}^{ab}$.¹¹ From eq (43) can be seen that the construction of R_3 is twice as expensive as the construction of τ_3 . For the Jacobian transformation the same terms have to be computed as for the ground state residual, but R_3 is contracted instead of τ_3 . Additionally,

the τ_3 amplitudes are required for a single term leading to an overall asymptotic scaling of $8n_{\text{v}}n_{\text{v}}^3n_{\text{o}}^3$ FLOP. It should be noted that the construction of Υ_{bDck} scales quadratically with the full system size. However, this term will not be significant compared to the other terms in the Jacobian transformation.

The transpose Jacobian transformation also scales with $8n_{\text{v}}n_{\text{v}}^3n_{\text{o}}^3$ FLOP, as the L_3 and τ_3 amplitudes need to be constructed and two contractions, each scaling as $2n_{\text{v}}n_{\text{v}}^3n_{\text{o}}^3$ FLOP, are needed. The final contractions contributing to the singles part of the transformed vector contains terms that scale quadratically with the full size of the system. However, these terms scale at most as $2n_{\text{v}}n_{\text{o}}n_{\text{v}}^2n_{\text{o}}$ FLOP and are therefore negligible compared to full CCSD.

To obtain core excited states core-valence separation is employed, where all non-zero elements of both the trial vector and the transformed vector need to contain at least one index corresponding to a core orbital.^{16,65,69} Therefore, in this implementation of the Jacobian transformations, we skip iterations in the loop over i, j, k if all indices correspond to valence orbitals. This reduces the scaling for both Jacobian transformations to $8n_{\text{v}}n_{\text{v}}^3n_{\text{o}}^2$.

As in the full CC3 code the EOM transition densities are constructed in a loop over the occupied indices and another loop over the virtual indices. We calculate all contributions to the density in a loop over the occupied indices, except for one contribution to the occupied-occupied block of the density which cannot be efficiently calculated in a loop over i, j, k .

$$D_{kl}^{m-0} = \frac{1}{2} \sum_{\substack{abc \\ ij}} \tilde{L}_{ijl}^{abc} \tau_{ijk}^{abc} \quad (46)$$

As shown in eq (46) for the occupied-occupied block of the left transition density, the triples amplitudes that are contracted differ in the occupied indices. Therefore, a triples loop over the virtual indices has to be used, in order to exploit the permutational symmetry of the triples amplitudes. This leads to an increase in contractions scaling as $2n_{\text{v}}n_{\text{v}}^3n_{\text{o}}^3$ FLOP. However, the triples amplitudes have to be reconstructed for the loop over a, b, c which also leads to a larger prefactor in the scaling. While the contractions inside the triple loops scale

linearly with the full system size, there exists one term in the right transition density, \tilde{D}^{0-m} , that requires storing a subblock of τ_2 scaling as $n_V n_O n_V n_O$ in memory. This is, however, not an issue as CCSD is used as lower level method where the full τ_2 array scaling as $n_V^2 n_O^2$ needs to be kept in memory.

Because the triples amplitudes have to be calculated twice the overall scaling to construct a single D^{m-0} amounts to $10n_V n_V^3 n_O^3$ FLOP. The construction of a single \tilde{D}^{0-m} totals $16n_V n_V^3 n_O^3$ FLOP, as the R_3 amplitudes are twice as expensive as the L_3 , and also the τ_3 and λ_3 amplitudes are required. For transition moments from the ground state, these densities only need to be computed once per state, compared to the iterative cost (per state) for the Jacobian transformations.

Results and Discussion

With the MLCC3 method, we can obtain excitation energies and oscillator strengths of CC3 quality at significantly reduced cost. We compare the MLCC3 results for oxygen core excitations of guanine to the CC3 results. The scaling with the size of the inactive space is shown for formaldehyde with up to six explicit water molecules. To show the capabilities of the method, the UV/VIS spectrum of azobenzene and a core excited state of betaine 30 with more than 1000 molecular orbitals are reported.

Guanine

A single core excited state of the oxygen atom of guanine is calculated with aug-cc-pCVDZ basis set on the oxygen atom and aug-cc-pVDZ on the remaining atoms using two Intel Xeon-Gold 6138 with 40 threads in total.⁸⁰⁻⁸² The results and timings per iteration are summarized in Table 1 for selected active spaces. The number of virtual orbitals is chosen to be 10 times larger than the number of occupied orbitals. Already with an active space comprising 10 occupied orbitals the excitation energies improve by 2 eV compared to CCSD

and the difference to CC3 is only 0.4 eV. Increasing the active space to 15 occupied orbitals the deviation from the CC3 results is below 0.2 eV. For 15 occupied orbitals the error of MLCC3 is below the expected error of CC3 for oxygen core excitations. For the smallest

Table 1: Timings in seconds to compute a core excited state from the oxygen atom of guanine at the CCSD and MLCC3 level with several active spaces. Timings are given, averaged over the number of iterations when solving for $\boldsymbol{\tau}$, $\boldsymbol{\lambda}$, \boldsymbol{R} and \boldsymbol{L} . Additionally, timings to construct the ground state density, \boldsymbol{D}^{0-0} , left transition density, \boldsymbol{D}^{m-0} , and right transition density, $\tilde{\boldsymbol{D}}^{0-m}$, are reported. Note that the MLCC3 and CC3 timings only comprise the triples part.

n_o/n_v	CCSD	MLCC3					CC3
		10/100	13/130	15/150	18/180	20/200	
ω [eV]	535.91	533.90	533.76	533.69	533.61	533.58	533.51
$f \times 100$	3.26	2.42	2.31	2.26	2.20	2.18	2.12
$\boldsymbol{\tau}$	15.49	3.03	10.72	24.93	70.31	125.74	2220.55
$\boldsymbol{\lambda}$	25.78	5.40	21.49	46.08	130.22	238.02	4157.37
\boldsymbol{R}	24.48	1.72	4.82	9.22	20.90	33.13	301.98
\boldsymbol{L}	23.62	1.86	5.27	9.83	22.59	36.58	317.90
\boldsymbol{D}^{0-0}	0.59	5.80	25.76	66.43	175.06	312.30	5147.35
\boldsymbol{D}^{m-0}	0.21	3.68	14.76	33.33	95.24	171.81	2340.44
$\tilde{\boldsymbol{D}}^{0-m}$	0.71	7.29	29.97	65.50	182.68	320.64	4638.42

active space in Table 1 the cost per iteration is much smaller than the CCSD timings. The CC3 contribution dominates inly in the construction of the densities, because CCSD densities scale as $\mathcal{O}(n_v^3 n_o^2)$ in contrast to $\mathcal{O}(n_v n_v^3 n_o^3)$ for MLCC3 densities. Considering active spaces with 13 and 15 occupied orbitals, the time spent in the MLCC3 part of the code is almost identical to the time in the CCSD code. The excited states are significantly cheaper with MLCC3, as CVS is implemented by skipping iterations in the i, j, k loop, effectively reducing the scaling to $\mathcal{O}(n_v n_v^3 n_o^2)$.

In Table 2 we report speed up compared to CC3. For terms scaling as $\mathcal{O}(n_v n_v^3 n_o^3)$ the speed up is calculated as,

$$S^{GS} = \frac{t_{CC3}^{it}}{t_{MLCC3}^{it}} \quad S_{theo}^{GS} = \frac{(n_o \times n_v)^3}{(n_o \times n_v)^3}, \quad (47)$$

Table 2: Speed up of MLCC3 compared to CC3 calculated according to equations 47 and 48. The first part shows the speed up for terms that scale asymptotically as $\mathcal{O}(n_V n_V^3 n_O^3)$ while the second part summarizes the speed up for terms with a cost of $\mathcal{O}(n_V n_V^3 n_O^2)$.

n_o	10	13	15	18	20
n_V	100	130	150	180	200
τ	732.9	207.1	89.1	31.6	17.7
λ	769.9	193.5	90.2	31.9	17.5
D^{0-0}	887.5	199.8	77.5	29.4	16.5
D^{m-0}	636.0	158.6	70.2	24.6	13.6
\tilde{D}^{0-m}	636.3	154.8	70.8	25.4	14.5
S_{theo}^{GS}	1079.1	223.6	94.7	31.7	16.9
R	175.6	62.7	32.6	14.5	9.1
L	170.9	60.3	32.3	14.1	8.7
S_{theo}^{ES}	276.7	74.5	36.4	14.6	8.7

while for core excited states the reduction in the scaling is given by,

$$S^{ES} = \frac{t_{CC3}^{it}}{t_{MLCC3}^{it}} \quad S_{theo}^{ES} = \frac{n_O^2 \times n_V^3}{n_O^2 \times n_V^3}. \quad (48)$$

It should be noted that only the dominating terms are included in this estimate, but terms with a lower scaling can be significant, especially for small active spaces. With an active space of 15 occupied orbitals a speed up of about 90 can be reached, while the deviation from the CC3 results is below 0.2 eV.

As we pursue a state-averaged approach in the determination of the active space, the performance is expected to deteriorate somewhat when more states are considered. Four core excited states of the oxygen atom of guanine are calculated with aug-cc-pCVDZ basis set on the oxygen atom and aug-cc-pVDZ on the remaining atoms.⁸⁰⁻⁸² The calculations were performed on two Intel Xeon E5-2699 v4 processors using 40 threads, so the timings are not directly comparable to Table 1.

Instead of specifying active spaces explicitly, we chose to use the CNTO threshold as defined in eq 34 and 35. For a more direct comparison the results of calculations performed

as above are tabulated in the SI (Table ??). Both the thresholds for the occupied and virtual orbital space are reduced from 10^{-1} to 10^{-6} while keeping both thresholds at the same magnitude. The size of the active spaces and the full size of the system are summarized in Table 3. By using the thresholds, the ratio between active virtual orbitals and active occupied orbitals reduces to approximately 7.

The excitation energies, ω , and oscillator strengths, f , are reported in Table 4. For a threshold of 10^{-1} the occupied orbital space consists only of a single orbital, such that the triples amplitudes are zero by definition. The results for this threshold are always identical to CCSD. The results of Table 4 are plotted in Figure 1 in addition to the CCSD and CC3

Table 3: Number of occupied and virtual orbitals in the active space for guanine for various CNTO thresholds. The CNTOs have been constructed from four core excited states obtained at the CCSD level of theory.

ξ	n_o	n_v
10^{-1}	1	4
10^{-2}	5	8
10^{-3}	16	56
10^{-4}	26	138
10^{-5}	29	208
10^{-6}	32	244
Full space	39	263

Table 4: First 4 excited states of guanine with MLCC3 for decreasing CNTO thresholds.

ξ	State 1		State 2		State 3		State 4	
	ω [eV]	$f \times 100$	ω [eV]	$f \times 100$	ω [eV]	$f \times 100$	ω [eV]	$f \times 100$
CCSD	535.9067	3.20	538.4340	0.12	539.3858	0.05	539.6794	0.08
10^{-2}	534.8780	2.80	536.3546	0.08	537.7091	0.02	537.8040	0.00
10^{-3}	533.9879	2.43	535.1010	0.07	535.6097	0.11	536.1425	0.00
10^{-4}	533.5776	2.17	534.5033	0.06	534.7363	0.15	535.3402	0.01
10^{-5}	533.5184	2.12	534.3886	0.05	534.6080	0.15	535.1326	0.01
10^{-6}	533.5107	2.12	534.3704	0.05	534.5925	0.15	535.0691	0.02
CC3	533.5091	2.12	534.3599	0.05	534.5888	0.15	535.0139	0.02

results, depicted by the horizontal lines. Increasing the active space improves the energies

until the error is below the expected error of the full CC3 method at a CNTO threshold of 10^{-4} . The oscillator strengths of the first and second state converge smoothly towards their CC3 values, however, larger jumps are found for the third and fourth state. These jumps are artifacts of the small active spaces, the plots in the SI show a smooth convergence towards the CC3 values. For the oscillator strengths the CCSD values have not been plotted as horizontal lines because they would overload the plot, and they coincide with the data points for $\xi = 10^{-1}$. Table 5 shows the timings of one iteration of the most expensive

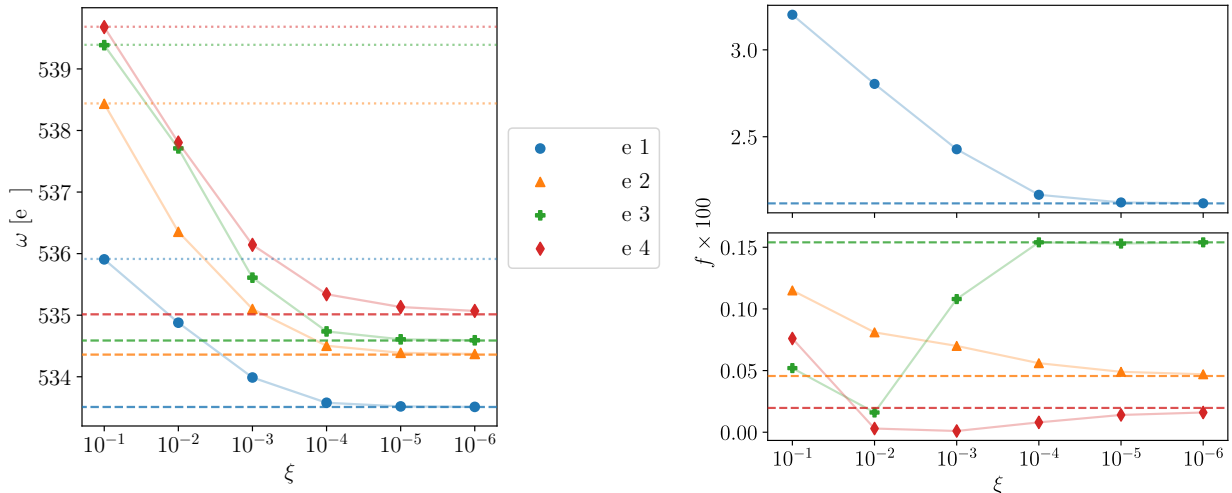


Figure 1: Convergence of the first four core excitation energies (left) and oscillator strengths (right) of guanine with CNTO threshold. Dashed lines are the CC3 results and dotted lines denote the CCSD values.

parts of the calculation of MLCC3 oscillator strengths. For thresholds below 10^{-4} the CC3 contribution is negligible when solving for ground and excited state amplitudes. However, the calculation of the EOM densities is already dominated by the CC3 part at $\xi = 10^{-3}$. Compared to the timings for solving the amplitudes the densities are still insignificant at a threshold of 10^{-3} . At 10^{-4} the CC3 contribution dominates all timings, but compared to a full CC3 calculation the cost per iteration is reduced by more than a factor of 30 for the ground state equations 20 for the excited states (SI Table ??). Even at 10^{-6} there is still a reduction of a factor of two, despite most orbitals being included in the active space.

Comparing Table 1 and 4, shows that the results with 20 occupied and 200 virtual orbitals

Table 5: Timings in seconds to compute four core excited states from the oxygen atom of guanine at the CCSD, CC3 and MLCC3 level with decreasing CNTO threshold. Timings are given, averaged over the number of iterations when solving for τ , λ , \mathbf{R} and \mathbf{L} . Additionally, timings to construct the ground state density, \mathbf{D}^{0-0} , left transition density, \mathbf{D}^{m-0} , and right transition density, $\tilde{\mathbf{D}}^{0-m}$, are reported. Note that the MLCC3 and CC3 timings only comprise the triples part.

	CCSD	MLCC3					CC3
		10^{-2}	10^{-3}	10^{-4}	10^{-5}	10^{-6}	
τ	22.8	0.08	2.75	133.79	704.15	1783.39	4180.2
λ	44.2	0.13	5.68	270.98	1414.40	3408.42	8593.9
\mathbf{R}	38.7	0.10	1.23	30.89	149.33	342.51	700.2
\mathbf{L}	43.3	0.12	1.31	32.27	145.30	318.53	702.0
\mathbf{D}^{0-0}	0.6	0.02	6.27	324.25	1658.26	4020.82	8765.3
\mathbf{D}^{m-0}	0.3	0.01	3.57	164.82	735.92	1662.66	3033.6
$\tilde{\mathbf{D}}^{0-m}$	1.2	0.06	7.39	330.58	1546.95	3647.72	7224.9

are slightly worse than the first excitation for $\xi = 10^{-4}$, although the latter includes only 6 more occupied but 62 less virtual orbitals. Therefore, we included calculations with a lower ratio between active virtual and occupied orbitals. Table 6 shows the results for these calculations, confirming that significantly less virtual orbitals are needed to obtain almost identical results. With 18 occupied and 130 virtual orbitals a speed up of up to 80 is achieved, and with 20 occupied and 130 virtual orbitals the speed up is still around 50 (SI Table ??).

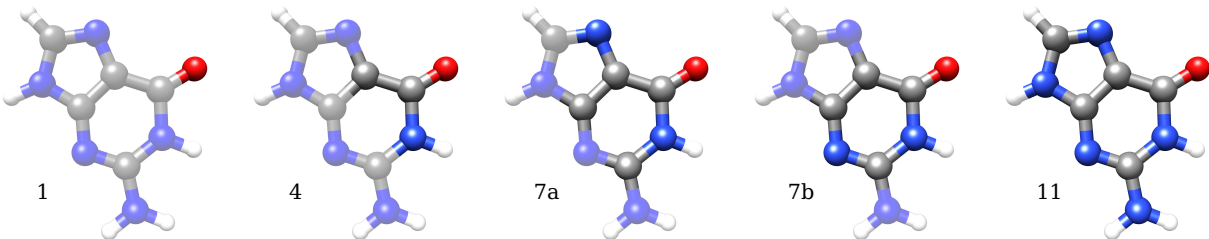


Figure 2: Geometry of guanine showing the active regions for which occupied Cholesky orbitals and PAOs have been constructed. The labels denote the number of active atoms and hydrogens are always inactive.

We have also performed some calculations with Cholesky occupied orbitals and PAOs for the virtual space. The active atoms are shown in Figure 2 as solid atoms and 10^{-2} was used as threshold for the Cholesky decomposition of the AO density. The size of the active

Table 6: Calculations of a single core excited state of guanine from the oxygen atom at the CCSD, CC3 and MLCC3 level with varying sizes of the active space. Excitation energies, ω , and oscillator strengths, f , as well as timings to construct the ground state density, \mathbf{D}^{0-0} , left transition density, \mathbf{D}^{m-0} , and right transition density, $\tilde{\mathbf{D}}^{0-m}$, are reported. Additionally timings are given, averaged over the number of iterations when solving for $\boldsymbol{\tau}$, $\boldsymbol{\lambda}$, \mathbf{R} and \mathbf{L} . Note that the MLCC3 and CC3 timings only comprise the triples part and that timings are given in seconds.

MLCC3						
n_o/n_v	16/160	18/130	18/150	18/180	20/130	20/200
ω [eV]	533.66	533.64	533.62	533.61	533.61	533.58
$f \times 100$	2.23	2.24	2.21	2.20	2.22	2.18
$\boldsymbol{\tau}$	40.09	28.09	41.22	70.31	38.32	125.74
$\boldsymbol{\lambda}$	70.96	53.86	76.78	130.22	73.14	238.02
\mathbf{R}	12.83	8.70	12.30	20.90	10.59	33.13
\mathbf{L}	13.43	9.69	13.23	22.59	11.88	36.58
\mathbf{D}^{0-0}	83.67	69.90	103.69	175.06	94.52	312.30
\mathbf{D}^{m-0}	48.37	38.19	59.63	95.24	50.33	171.81
$\tilde{\mathbf{D}}^{0-m}$	90.03	75.51	111.44	182.68	95.11	320.64

Table 7: Number of occupied and virtual orbitals in the active spaces constructed using Cholesky orbitals and PAOs for guanine.

System label (Figure 2)	n_o	n_v
1	5	26
4	23	92
7a	33	158
7b	33	158
11	39	245
Full space	39	263

Table 8: First 4 excited states of Guanine with MLCC3 calculated with active spaces constructed from Cholesky orbitals and PAOs.

	State 1		State 2		State 3		State 4	
	ω [eV]	$f \times 100$	ω [eV]	$f \times 100$	ω [eV]	$f \times 100$	ω [eV]	$f \times 100$
1	534.6250	2.81	537.0755	0.13	538.2042	0.39	538.2714	0.28
4	533.8427	2.37	534.9479	0.07	535.9413	0.05	536.0856	0.15
7a	533.5901	2.17	534.6548	0.06	534.9312	0.16	535.4104	0.04
7b	533.6082	2.19	534.6045	0.06	534.8809	0.16	535.4454	0.03
11	533.5110	2.12	534.4149	0.05	534.5932	0.15	535.0960	0.02
CC3	533.5091	2.12	534.3599	0.05	534.5888	0.15	535.01394	0.02

spaces are summarized in Table 7 and the results are reported in Table 8. As shown in

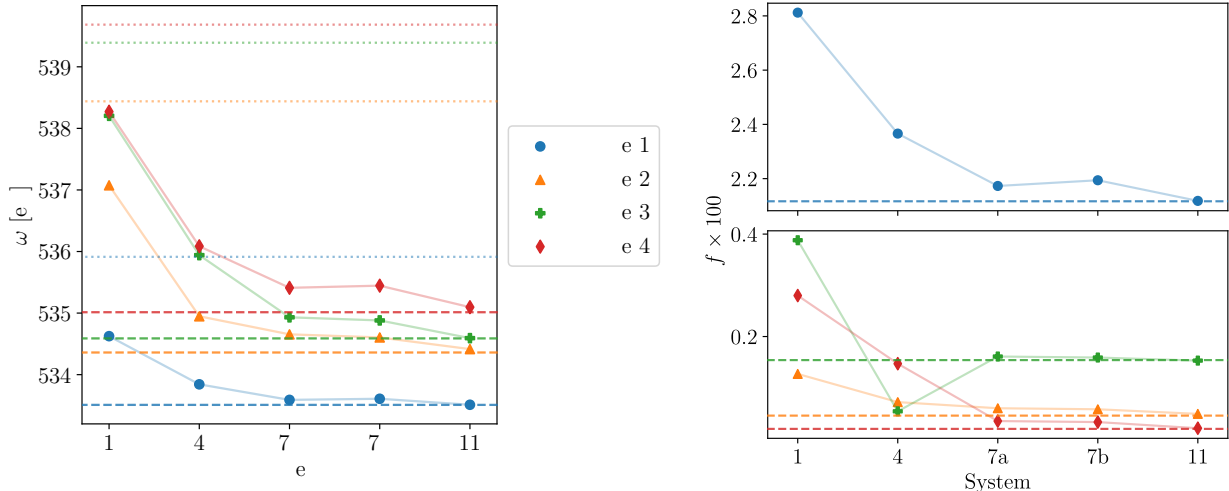


Figure 3: Convergence of the first four core excitation energies (left) and oscillator strengths (right) of guanine for the five active spaces in Figure 2. Dashed lines are the CC3 results and dotted lines denote the CCSD values.

Figure 3 the excitation energies are already significantly improved when only the oxygen is included in the active space. However, the size of the active spaces also increases much faster, because all the atoms contribute to the π -system. Despite the active spaces being larger, the performance of the Cholesky/PAOs is worse than calculations with a similarly large active space consisting of CNTOs. The reason for the poor performance of these active spaces is that we split up the π -system. Additionally, the CC3 excitation vectors consist of multiple similarly large amplitudes which need to be described accurately by the active space. An active space consisting of CNTOs is better suited to describe such excited states.

Formaldehyde in water

To investigate the scaling with the size of the inactive orbital space we consider formaldehyde with several explicit water molecules. The calculations were performed on two Intel Xeon-Gold 6138 using 40 threads. Comparing excitation energy and oscillator strength is not constructive for this system, because CCSD and CC3 already almost coincide for the first excited state. The geometry for formaldehyde with six water molecules is reported in the

SI; it has been adapted from a geometry with 10 water molecules from Ref. 83. The other geometries are generated by subsequently removing water molecules, starting with the last one. For a proper investigation of solvent effects, randomized geometries would have to be extracted from a molecular dynamics simulation and the results would have to be averaged.⁸⁴

For all calculations we used a aug-cc-pVTZ basis set and the active space comprises 8 occupied and 136 virtual orbitals. The sizes of the systems considered are summarized in Table 9.

Table 9: Number of occupied and virtual orbitals for formaldehyde with increasing number of water molecules with aug-cc-pVTZ basis set.

System #H ₂ O	aug-cc-pVTZ	
	n_O	n_V
1	13	217
2	18	304
3	23	391
4	28	478
5	33	565
6	38	652

Figure 4 shows the timing breakdown for the MLCC3 contribution in the calculation of EOM oscillator strengths. As expected the timings for every quantity increase linearly with the number of water molecules added to the system, implying the terms scaling quadratically with the full system size are negligible.

Azobenzene

In the aug-cc-pVDZ basis, azobenzene has 48 occupied and 364 virtual orbitals. On two Intel Xeon E5-2699 v4 processors using 40 threads a single iteration of the CC3 ground state equations takes 6 hours. As the Jacobian transformations are twice as expensive per state, a CC3 calculation of 10 excited states is costly.

By using an active space containing 34 occupied and 238 virtual orbitals, the time per iteration of the ground state equations reduced to 36 minutes. In figure 5, the spectra

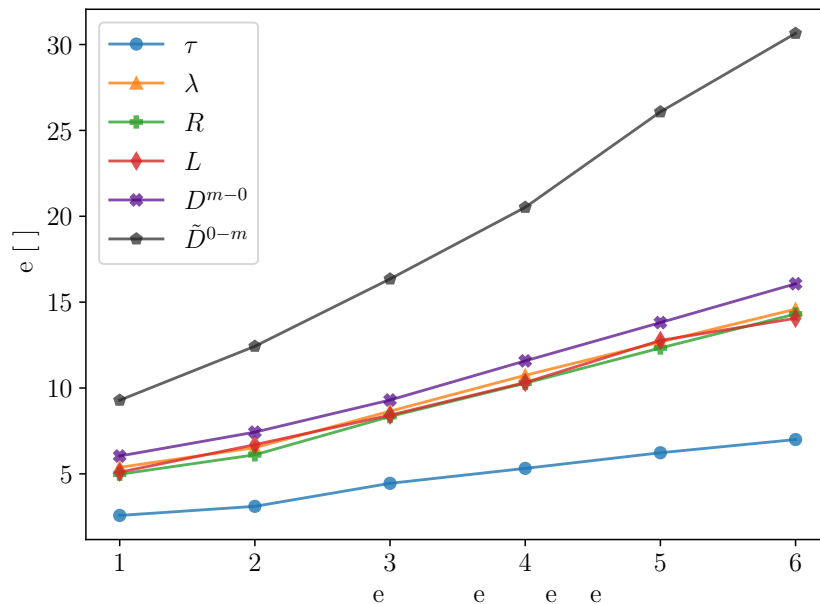


Figure 4: Average time to calculate one transition density or one iteration solving for τ , λ , L and R with increasing number of water molecules in the inactive space.

calculated at the CCSD and MLCC3 level of theory are shown together with the experimental results. While the CCSD results are significantly blue shifted, the broadened MLCC3 values match very well with the experimental bands at 300 nm and 220 nm. The very broad band at around 450 nm is not reproduced, but an almost dark excitation is found around 420 nm. CCSD predicts this latter excitation to be at 400 nm instead.

Betaine 30

To demonstrate the capabilities of our MLCC3 implementation, we consider the first core excitation from the oxygen atom in betaine 30. The geometry is shown in Figure 6. The system comprises 145 occupied and 992 virtual orbitals using a aug-cc-pCVDZ basis set for the oxygen atom, aug-cc-pVDZ for carbon and nitrogen atoms and cc-pVDZ for hydrogen atoms. In Table 10 we report the excitation energy and oscillator strengths for CCSD and MLCC3 using three active CNTO spaces of increasing size. Using CCSD both the excitation energy and especially the oscillator strength are overestimated compared to the MLCC3

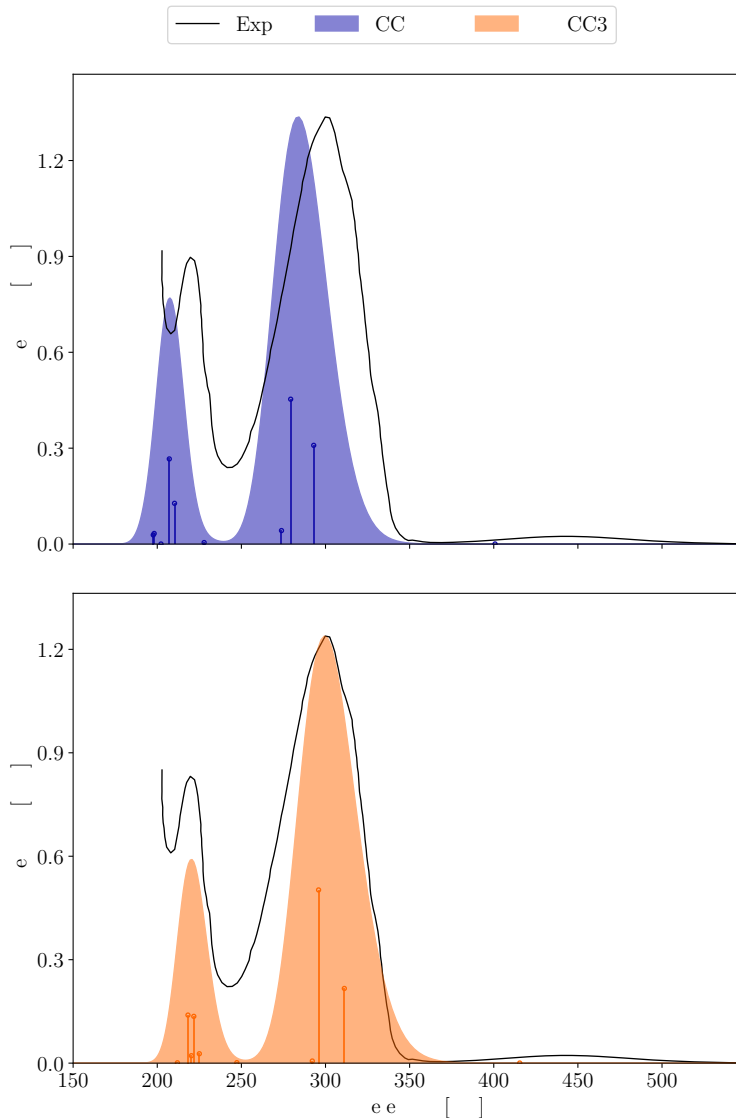


Figure 5: UV-VIS absorption spectrum of azobenzene calculated with CCSD and MLCC3 employing aug-cc-pVDZ basis set.⁸⁰ The theoretical stick spectrum is broadened using Gaussian functions with fwhm of 0.5 eV and the experimental data is taken from Ref. 85.

results. Increasing the size of the active space from 20 occupied and 200 virtual CNTOs to 25 occupied and 250 virtual orbitals, only changes the excitation energy by 0.3 eV. Therefore, we can assume that the MLCC3 results are within the expected error range of a full CC3 calculation.

Due to the significant size of the system the time spent calculating the contribution of the triple excitations is small compared to the timings of CCSD, as shown in Table 11. For the

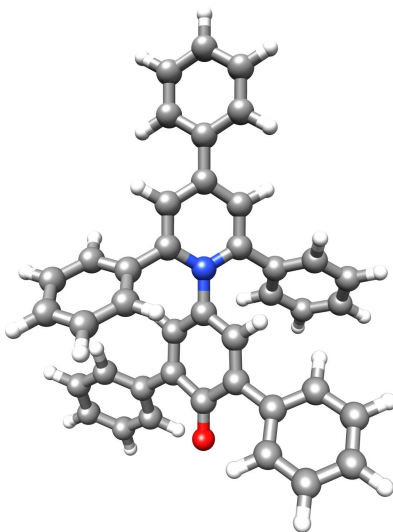


Figure 6: Geometry of the betaine 30.

Table 10: First core excitation from the oxygen atom calculated at the CCSD level of theory and MLCC3 with increasing number of CNTOs in the active space.

	ω [eV]	$f \times 100$	n_o	n_v
CCSD	535.12	2.74		
MLCC3	531.50	0.67	20	200
MLCC3	531.29	0.63	25	200
MLCC3	531.32	0.63	25	250

densities the triples contribution dominates, however, the time used to construct densities is still small compared to determining the ground and excited states.

Conclusion

The multilevel CC3 method provides a framework, with which intensive molecular properties can be calculated at an accuracy approaching that of the CC3 method. For sufficiently large inactive spaces the computational cost will tend towards that of CCSD. Compared to Cholesky PAOs, CNTOs provide smaller orbital spaces without sacrificing accuracy. However, the cost of constructing CNTOs is significant, as the CCSD ground and excited state equations need to be solved.

Table 11: Timings in minutes to compute a core excited state from the oxygen atom of betaine 30 at the CCSD and MLCC3 level with several active spaces. Timings are given, averaged over the number of iterations when solving for $\boldsymbol{\tau}$, $\boldsymbol{\lambda}$, \boldsymbol{R} and \boldsymbol{L} . Additionally, timings to construct the ground state density, \boldsymbol{D}^{0-0} , left transition density, \boldsymbol{D}^{m-0} , and right transition density, $\tilde{\boldsymbol{D}}^{0-m}$, are reported. Note that the MLCC3 and CC3 timings only comprise the triples part.

n_o/n_v	CCSD	MLCC3		
		20/200	25/200	25/250
$\boldsymbol{\tau}$	73.2	3.1	5.6	10.7
$\boldsymbol{\lambda}$	143.5	6.4	12.0	21.4
\boldsymbol{R}	122.6	1.2	1.7	2.8
\boldsymbol{L}	130.8	1.3	1.9	3.2
\boldsymbol{D}^{0-0}	0.5	8.0	14.6	28.6
\boldsymbol{D}^{m-0}	0.5	5.2	9.4	18.3
$\tilde{\boldsymbol{D}}^{0-m}$	1.0	9.1	16.5	31.2

There is some ambiguity regarding the selection of the active space using CNTOs. We can either specify the number of occupied and virtual orbitals explicitly or use a cutoff, ξ , and include the orbitals whose eigenvalues sum up to $1 - \xi$. The first approach gives great flexibility, but several calculations are typically needed to confirm that the excitation energies actually converged. Using a cutoff on the other hand is a more blackbox approach, as $\xi = 10^{-4}$ gives accurate results, but the active spaces can become larger than required. Further benchmarking, especially on larger systems, is needed to obtain a rule of thumb for the selection of an active space.

Two bottlenecks were identified that limit the size of the systems we can treat: First, the convergence behaviour of the solvers is diminished, due to the change of the orbital basis. The start guess could be improved by transforming the CCSD amplitudes from canonical MOs to the CNTO basis.

For large systems with several hundreded to a thousand MOs, CCSD becomes a bottleneck and another layer could be introduced at the CCS level of theory. For the multilevel CC3 model with CC3 in CCSD in CCS, it has to be investigated how the orbital space is set up effectively, as NTOs obtained from CCS will not provide a suitable active space. One

possibility could be the approximated CNTOs introduced by Baudin and Kristensen, or CNTOs obtained from a MLCCSD calculation.⁸⁶

Acknowledgement

We acknowledge computing resources through UNINETT Sigma2 - the National Infrastructure for High Performance Computing and Data Storage in Norway, through project number NN2962k. We acknowledge funding from the Marie Skłodowska-Curie European Training Network “COSINE – COmputational Spectroscopy In Natural sciences and Engineering”, Grant Agreement No. 765739 and the Research Council of Norway through FRINATEK projects 263110, CCGPU, and 275506, TheoLight.

References

- (1) Helgaker, T.; Coriani, S.; Jørgensen, P.; Kristensen, K.; Olsen, J.; Ruud, K. Recent Advances in Wave Function-Based Methods of Molecular-Property Calculations. *Chem. Rev.* **2012**, *112*, 543–631.
- (2) Koch, H.; Jørgensen, P. Coupled cluster response functions. *J. Chem. Phys.* **1990**, *93*, 3333–3344.
- (3) Pedersen, T. B.; Koch, H. Coupled cluster response functions revisited. *J. Chem. Phys.* **1997**, *106*, 8059–8072.
- (4) Norman, P.; Dreuw, A. Simulating X-ray Spectroscopies and Calculating Core-Excited States of Molecules. *Chem. Rev.* **2018**, *118*, 7208–7248.
- (5) Myhre, R. H.; Wolf, T. J. A.; Cheng, L.; Nandi, S.; Coriani, S.; Gühr, M.; Koch, H. A theoretical and experimental benchmark study of core-excited states in nitrogen. *J. Chem. Phys.* **2018**, *148*, 064106.
- (6) Liu, J.; Matthews, D.; Coriani, S.; Cheng, L. Benchmark Calculations of K-Edge Ionization Energies for First-Row Elements Using Scalar-Relativistic Core-Valence-Separated Equation-of-Motion Coupled-Cluster Methods. *J. Chem. Theory Comput.* **2019**, *15*, 1642–1651.
- (7) Oosterbaan, K. J.; White, A. F.; Head-Gordon, M. Non-Orthogonal Configuration Interaction with Single Substitutions for Core-Excited States: An Extension to Doublet Radicals. *J. Chem. Theory Comput.* **2019**, *15*, 2966–2973.
- (8) Myhre, R. H.; Coriani, S.; Koch, H. X-ray and UV Spectra of Glycine within Coupled Cluster Linear Response Theory. *J. Phys. Chem. A* **2019**, *123*, 9701–9711.
- (9) Christiansen, O.; Koch, H.; Jørgensen, P. Perturbative triple excitation corrections to

- coupled cluster singles and doubles excitation energies. *J. Chem. Phys.* **1996**, *105*, 1451–1459.
- (10) Noga, J.; Bartlett, R. J. The full CCSDT model for molecular electronic structure. *J. Chem. Phys.* **1987**, *86*, 7041–7050.
- (11) Helgaker, T.; Jørgensen, P.; Olsen, J. *Molecular electronic-structure theory*; wiley, 2014; pp 1–908.
- (12) Koch, H.; Kobayashi, R.; Sánchez de Merás, A.; Jørgensen, P. Calculation of size-intensive transition moments from the coupled cluster singles and doubles linear response function. *J. Chem. Phys.* **1994**, *100*, 4393–4400.
- (13) Noga, J.; Bartlett, R. J.; Urban, M. Towards a full CCSDT model for electron correlation. CCSDT-n models. *Chem. Phys. Lett.* **1987**, *134*, 126 – 132.
- (14) Christiansen, O.; Koch, H.; Jørgensen, P. Response functions in the CC3 iterative triple excitation model. *J. Chem. Phys.* **1995**, *103*, 7429–7441.
- (15) Hald, K.; Jørgensen, P.; Christiansen, O.; Koch, H. Implementation of electronic ground states and singlet and triplet excitation energies in coupled cluster theory with approximate triples corrections. *J. Chem. Phys.* **2002**, *116*, 5963–5970.
- (16) Paul, A. C.; Myhre, R. H.; Koch, H. New and Efficient Implementation of CC3. *J. Chem. Theory Comput* **2021**, *17*, 126.
- (17) Kowalski, K.; Piecuch, P. New coupled-cluster methods with singles, doubles, and non-iterative triples for high accuracy calculations of excited electronic states. *J. Chem. Phys.* **2004**, *120*, 1715–1738.
- (18) Stanton, J. F.; Gauss, J. A simple correction to final state energies of doublet radicals described by equation-of-motion coupled cluster theory in the singles and doubles approximation. *Theor. Chim. Acta* **1996**, *93*, 303–313.

- (19) Saeh, J. C.; Stanton, J. F. Application of an equation-of-motion coupled cluster method including higher-order corrections to potential energy surfaces of radicals. *J. Chem. Phys.* **1999**, *111*, 8275–8285.
- (20) Matthews, D. A.; Stanton, J. F. A new approach to approximate equation-of-motion coupled cluster with triple excitations. *J. Chem. Phys.* **2016**, *145*, 124102.
- (21) A comparison of excited state properties for iterative approximate triples linear response coupled cluster methods. *Chem. Phys. Lett.* **2001**, *347*, 499–504.
- (22) Sauer, S. P.; Schreiber, M.; Silva-Junior, M. R.; Thiel, W. Benchmarks for electronically excited states: a comparison of noniterative and iterative triples corrections in linear response coupled cluster methods: CCSDR(3) versus CC3. *J. Chem. Theory Comput.* **2009**, *5*, 555–564.
- (23) Pulay, P. Localizability of dynamic electron correlation. *Chem. Phys. Lett.* **1983**, *100*, 151–154.
- (24) Saebø, S.; Pulay, P. Local treatment of electron correlation. *Annu. Rev. Phys. Chem.* **1993**, *44*, 213–236.
- (25) Sæbø, S.; Pulay, P. Local configuration interaction: An efficient approach for larger molecules. *Chem. Phys. Lett.* **1985**, *113*, 13–18.
- (26) Saebø, S.; Pulay, P. Fourth-order Møller-Plessett perturbation theory in the local correlation treatment. I. Method. *J. Chem. Phys.* **1986**, *86*, 914–922.
- (27) Saebø, S.; Pulay, P. The local correlation treatment. II. Implementation and tests. *J. Chem. Phys.* **1988**, *88*, 1884–1890.
- (28) Hampel, C.; Werner, H. J. Local treatment of electron correlation in coupled cluster theory. *J. Chem. Phys.* **1996**, *104*, 6286–6297.

- (29) Schütz, M.; Werner, H. J. Local perturbative triples correction (T) with linear cost scaling. *Chem. Phys. Lett.* **2000**, *318*, 370–378.
- (30) Schütz, M. Low-order scaling local electron correlation methods. III. Linear scaling local perturbative triples correction (T). *J. Chem. Phys.* **2000**, *113*, 9986–10001.
- (31) Neese, F.; Wennmohs, F.; Hansen, A. Efficient and accurate local approximations to coupled-electron pair approaches: An attempt to revive the pair natural orbital method. *J. Chem. Phys.* **2009**, *130*, 114108.
- (32) Neese, F.; Hansen, A.; Liakos, D. G. Efficient and accurate approximations to the local coupled cluster singles doubles method using a truncated pair natural orbital basis. *J. Chem. Phys.* **2009**, *131*, 64103.
- (33) Riplinger, C.; Sandhoefer, B.; Hansen, A.; Neese, F. Natural triple excitations in local coupled cluster calculations with pair natural orbitals. *J. Chem. Phys.* **2013**, *139*, 134101.
- (34) Frank, M. S.; Schmitz, G.; Hättig, C. Implementation of the iterative triples model CC3 for excitation energies using pair natural orbitals and Laplace transformation techniques. *J. Chem. Phys.* **2020**, *153*, 34109.
- (35) Korona, T.; Werner, H. J. Local treatment of electron excitations in the EOM-CCSD method. *J. Chem. Phys.* **2003**, *118*, 3006–3019.
- (36) Kats, D.; Korona, T.; Schütz, M. Local CC2 electronic excitation energies for large molecules with density fitting. *J. Chem. Phys.* **2006**, *125*, 244110.
- (37) Crawford, T. D.; Kumar, A.; Bazanté, A. P.; Di Remigio, R. Reduced-scaling coupled cluster response theory: Challenges and opportunities. *Wiley Interdiscip. Rev. Comput. Mol. Sci.* **2019**, *9*.

- (38) Kats, D.; Schütz, M. A multistate local coupled cluster CC2 response method based on the Laplace transform. *J. Chem. Phys.* **2009**, *131*, 64107.
- (39) Helmich, B.; Hättig, C. A pair natural orbital implementation of the coupled cluster model CC2 for excitation energies. *J. Chem. Phys.* **2013**, *139*, 84114.
- (40) Dutta, A. K.; Neese, F.; Izsák, R. Towards a pair natural orbital coupled cluster method for excited states. *J. Chem. Phys.* **2016**, *145*, 34102.
- (41) Dutta, A. K.; Nooijen, M.; Neese, F.; Izsák, R. Exploring the Accuracy of a Low Scaling Similarity Transformed Equation of Motion Method for Vertical Excitation Energies. *J. Chem. Theory Comput.* **2018**, *14*, 72–91.
- (42) Warshel, A.; Karplus, M. Calculation of Ground and Excited State Potential Surfaces of Conjugated Molecules.1 I. Formulation and Parametrization. *J. Am. Chem. Soc.* **1972**, *94*, 5612–5625.
- (43) Warshel, A.; Levitt, M. Theoretical studies of enzymic reactions: Dielectric, electrostatic and steric stabilization of the carbonium ion in the reaction of lysozyme. *J. Mol. Biol.* **1976**, *103*, 227–249.
- (44) Field, M. J.; Bash, P. A.; Karplus, M. A combined quantum mechanical and molecular mechanical potential for molecular dynamics simulations. *J. Comput. Chem.* **1990**, *11*, 700–733.
- (45) Lin, H.; Truhlar, D. G. QM/MM: what have we learned, where are we, and where do we go from here? *Theor Chem Acc* **2007**, *117*, 185–199.
- (46) Senn, H. M.; Thiel, W. QM/MM methods for biomolecular systems. 2009; www.angewandte.org.
- (47) Scheurer, M.; Herbst, M. F.; Reinholdt, P.; Olsen, J. M. H.; Dreuw, A.; Kongsted, J. Polarizable Embedding Combined with the Algebraic Diagrammatic Construction: Tack-

- ling Excited States in Biomolecular Systems. *J. Chem. Theory Comput.* **2018**, *14*, 4870–4883.
- (48) Wesolowski, T. A.; Warshel, A. Frozen density functional approach for ab initio calculations of solvated molecules. *J. Phys. Chem.* **1993**, *97*, 8050–8053.
- (49) Neugebauer, J.; Jacob, C. R.; Wesolowski, T. A.; Baerends, E. J. An explicit quantum chemical method for modeling large solvation shells applied to aminocoumarin C151. *J. Phys. Chem. A* **2005**, *109*, 7805–7814.
- (50) Cortona, P. Self-consistently determined properties of solids without band-structure calculations. *Phys. Rev. B* **1991**, *44*, 8454–8458.
- (51) Jacob, C. R.; Neugebauer, J. Subsystem density-functional theory. **2014**, *4*.
- (52) Humbel, S.; Sieber, S.; Morokuma, K. The IMOMO method: Integration of different levels of molecular orbital approximations for geometry optimization of large systems: Test for n-butane conformation and SN2 reaction: RCl+Cl-. *J. Chem. Phys.* **1996**, *105*, 1959–1967.
- (53) Svensson, M.; Humbel, S.; Froese, R. D.; Matsubara, T.; Sieber, S.; Morokuma, K. *ONIOM: A multilayered integrated MO + MM method for geometry optimizations and single point energy predictions. A test for Diels-Alder reactions and Pt(P(t-Bu)₃)₂ + H₂ oxidative addition*; 1996; Vol. 100; pp 19357–19363.
- (54) Mata, R. A.; Werner, H. J.; Schütz, M. Correlation regions within a localized molecular orbital approach. *J. Chem. Phys.* **2008**, *128*, 5691.
- (55) Oliphant, N.; Adamowicz, L. Multireference coupled-cluster method using a single-reference formalism. *J. Chem. Phys.* **1991**, *94*, 1229–1235.

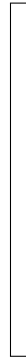
- (56) Piecuch, P.; Oliphant, N.; Adamowicz, L. A state-selective multireference coupled-cluster theory employing the single-reference formalism. *J. Chem. Phys.* **1993**, *99*, 1875–1900.
- (57) Kállay, M.; Szalay, P. G.; Surján, P. R. A general state-selective multireference coupled-cluster algorithm. *J. Chem. Phys.* **2002**, *117*, 980–990.
- (58) Olsen, J. The initial implementation and applications of a general active space coupled cluster method. *J. Chem. Phys.* **2000**, *113*, 7140–7148.
- (59) Köhn, A.; Olsen, J. Coupled-cluster with active space selected higher amplitudes: Performance of seminatural orbitals for ground and excited state calculations. *J. Chem. Phys.* **2006**, *125*, 184103.
- (60) Myhre, R. H.; Sánchez De Merás, A. M.; Koch, H. The extended CC2 model ECC2. *Mol. Phys.* **2013**, *111*, 1109–1118.
- (61) Myhre, R. H.; Sánchez De Merás, A. M.; Koch, H. Multi-level coupled cluster theory. *J. Chem. Phys.* **2014**, *141*, 224105.
- (62) Myhre, R. H.; Koch, H. The multilevel CC3 coupled cluster model. *J. Chem. Phys.* **2016**, *145*, 44111.
- (63) Aquilante, F.; Pedersen, T. B.; de Merás, A. S.; Koch, H. Fast noniterative orbital localization for large molecules. *J. Chem. Phys.* **2006**, *125*, 174101.
- (64) Høyvik, I.-M.; Myhre, R. H.; Koch, H. Correlated natural transition orbitals for core excitation energies in multilevel coupled cluster models. *J. Chem. Phys.* **2017**, *146*, 144109.
- (65) Myhre, R. H.; Coriani, S.; Koch, H. Near-Edge X-ray Absorption Fine Structure within Multilevel Coupled Cluster Theory. *J. Chem. Theory Comput.* **2016**, *12*, 2633–2643.

- (66) Folkestad, S. D.; Koch, H. Equation-of-Motion MLCCSD and CCSD-in-HF Oscillator Strengths and Their Application to Core Excitations. *J. Chem. Theory Comput.* **2020**, *16*, 6869–6879.
- (67) Cederbaum, L. S. Many-body theory of multiple core holes. *Phys. Rev. A* **1987**, *35*, 622–631.
- (68) Wenzel, J.; Wormit, M.; Dreuw, A. Calculating core-level excitations and x-ray absorption spectra of medium-sized closed-shell molecules with the algebraic-diagrammatic construction scheme for the polarization propagator. *J. Comput. Chem.* **2014**, *35*, 1900–1915.
- (69) Coriani, S.; Koch, H. Communication: X-ray absorption spectra and core-ionization potentials within a core-valence separated coupled cluster framework. *J. Chem. Phys.* **2015**, *143*.
- (70) Stanton, J. F.; Bartlett, R. J. The equation of motion coupled-cluster method. A systematic biorthogonal approach to molecular excitation energies, transition probabilities, and excited state properties. *J. Chem. Phys.* **1993**, *98*, 7029–7039.
- (71) Stanton, J. F. Separability properties of reduced and effective density matrices in the equation-of-motion coupled cluster method. *J. Chem. Phys.* **1994**, *101*, 8928–8937.
- (72) Levchenko, S. V.; Wang, T.; Krylov, A. I. Analytic gradients for the spin-conserving and spin-flipping equation-of-motion coupled-cluster models with single and double substitutions. *J. Chem. Phys.* **2005**, *122*, 224106.
- (73) Sánchez De Merás, A. M.; Koch, H.; Cuesta, I. G.; Boman, L. Cholesky decomposition-based definition of atomic subsystems in electronic structure calculations. *J. Chem. Phys.* **2010**, *132*, 204105.

- (74) Folkestad, S. D.; Kjøenstad, E. F.; Goletto, L.; Koch, H. Multilevel CC2 and CCSD in Reduced Orbital Spaces: Electronic Excitations in Large Molecular Systems. *J. Chem. Theory Comput.* **2021**, *17*, 714–726.
- (75) Goletto, L.; Giovannini, T.; Folkestad, S. D.; Koch, H. Combining multilevel Hartree-Fock and multilevel coupled cluster approaches with molecular mechanics: a study of electronic excitations in solutions. *Phys. Chem. Chem. Phys.* **2021**, *23*, 4413–4425.
- (76) Folkestad, S. D.; Kjøenstad, E. F.; Myhre, R. H.; Andersen, J. H.; Balbi, A.; Coriani, S.; Giovannini, T.; Goletto, L.; Haugland, T. S.; Hutcheson, A.; Høyvik, I.-M.; Moitra, T.; Paul, A. C.; Scavino, M.; Skeidsvoll, A. S.; Tveten, Å. H.; Koch, H. eT 1.0: An open source electronic structure program with emphasis on coupled cluster and multilevel methods. *J. Chem. Phys.* **2020**, *152*, 184103.
- (77) Rendell, A. P.; Lee, T. J.; Komornicki, A. A parallel vectorized implementation of triple excitations in CCSD(T): application to the binding energies of the AlH₃, AlH₂F, AlHF₂ and AlF₃ dimers. *Chem. Phys. Lett.* **1991**, *178*, 462–470.
- (78) Matthews, D. A.; Gauss, J.; Stanton, J. F. Revisitation of Nonorthogonal Spin Adaptation in Coupled Cluster Theory. *J. Chem. Theory Comput.* **2013**, *9*, 2567–2572.
- (79) Matthews, D. A.; Stanton, J. F. Non-orthogonal spin-adaptation of coupled cluster methods: A new implementation of methods including quadruple excitations. *J. Chem. Phys.* **2015**, *142*, 064108.
- (80) Kendall, R. A.; Dunning, T. H.; Harrison, R. J. Electron affinities of the first-row atoms revisited. Systematic basis sets and wave functions. *J. Chem. Phys.* **1992**, *96*, 6796–6806.
- (81) Woon, D. E.; Dunning, T. H. Gaussian basis sets for use in correlated molecular calculations. V. Core-valence basis sets for boron through neon. *J. Chem. Phys.* **1995**, *103*, 4572–4585.

- (82) Dunning, T. H. Gaussian basis sets for use in correlated molecular calculations. I. The atoms boron through neon and hydrogen. *J. Chem. Phys.* **1989**, *90*, 1007–1023.
- (83) Folkestad, S. D.; Koch, H. Multilevel CC2 and CCSD Methods with Correlated Natural Transition Orbitals. *J. Chem. Theory Comput.* **2020**, *16*, 179–189.
- (84) Giovannini, T.; Riso, R. R.; Ambrosetti, M.; Puglisi, A.; Cappelli, C. Electronic transitions for a fully polarizable QM/MM approach based on fluctuating charges and fluctuating dipoles: Linear and corrected linear response regimes. *J. Chem. Phys.* **2019**, *151*, 174104.
- (85) den Hertog, H. J.; Combé, W. P. Reactivity of 4-nitropyridine-N-oxide: Preparation of 4-substituted derivatives of pyridine-N-oxide and pyridine. *Recl. des Trav. Chim. des Pays-Bas* **1952**, *71*, 1145–1151.
- (86) Baudin, P.; Kristensen, K. Correlated natural transition orbital framework for low-scaling excitation energy calculations (CorNFLEx). *J. Chem. Phys.* **2017**, *146*, 214114.

Graphical TOC Entry



Supporting information for *Oscillator strengths in the framework of equation-of-motion multilevel CC3*

Alexander C. Paul,[†] Sarai D. Folkestad,[†] Rolf H. Myhre,[†] and Henrik Koch^{*,†,‡}

[†]*Department of Chemistry, Norwegian University of Science and Technology, NTNU, 7491 Trondheim, Norway*

[‡]*Scuola Normale Superiore, Piazza dei Cavalieri 7, 56126 Pisa, Italy*

E-mail: henrik.koch@sns.it

Supporting Information Available

Here we report equations to construct the MLCC3 ground state residual, Jacobian transformations and transition densities. For a concise notation we define

$$\Delta_{ai,bj} = 1 + \delta_{ij}\delta_{ab} \quad (1)$$

$$\bar{R}_{ij}^{ab} = \Delta_{ai,bj}R_{ij}^{ab}. \quad (2)$$

For a given covariant doubles amplitude or residual X_{ij}^{ab} the contravariant quantity is defined as

$$\tilde{X}_{ij}^{ab} = 2X_{ij}^{ab} - X_{ij}^{ba} \quad (3)$$

and for a triples amplitude X_{ijk}^{abc}

$$\tilde{X}_{ijk}^{abc} = 4X_{ijk}^{abc} - 2X_{jik}^{bac} - 2X_{kji}^{cba} - 2X_{ikj}^{acb} + X_{kij}^{cab} + X_{jki}^{bca} \quad (4)$$

The contributions to the contravariant ground state residual $\tilde{\Omega}$ are listed below.

$$\tau_{ijk}^{abc} = -(\varepsilon_{ijk}^{abc})^{-1} P_{ijk}^{abc} \left(\sum_D \tau_{ij}^{aD} g_{bDck} - \sum_l \tau_{iL}^{ab} g_{Ljck} \right) \quad (5)$$

$$\tilde{\Omega}_i^a += \sum_{\substack{bc \\ jk}} \tilde{\tau}_{ijk}^{abc} g_{jbkc} \quad (6)$$

$$\tilde{\Omega}_{ij}^{ab} += P_{ij}^{ab} \sum_{\substack{c \\ k}} \tilde{\tau}_{ijk}^{abc} F_{kc} \quad (7)$$

$$\tilde{\Omega}_{iL}^{ab} -= P_{iL}^{ab} \sum_{\substack{c \\ jk}} \tilde{\tau}_{ijk}^{abc} g_{jLkc} \quad (8)$$

$$\tilde{\Omega}_{ij}^{aD} += P_{ij}^{aD} \sum_{\substack{bc \\ jk}} \tilde{\tau}_{ijk}^{abc} g_{Dbkc} \quad (9)$$

The Jacobian transformation of a trial vector \mathbf{R} consists of the following terms, where $\tilde{\rho}$

denotes the contravariant of the transformed vector.

$$\Upsilon_{kc} = \sum_L^D (2g_{kcLD} - g_{kDLc}) R_L^D \quad (10)$$

$$\Upsilon_{bDck} = \sum_E R_k^E g_{bDcE} - \sum_M (R_M^b g_{MDck} + R_M^c g_{bDMk}) \quad (11)$$

$$\Upsilon_{Ljck} = \sum_E (R_j^E g_{LEck} + R_k^E g_{Ljce}) - \sum_M R_M^c g_{LjMk} \quad (12)$$

$$R_{ijk}^{abc} = -\frac{1}{\varepsilon_{ijk}^{abc} - \omega} P_{ijk}^{abc} \left(\sum_D \bar{R}_{ij}^{aD} g_{bDck} - \sum_L \bar{R}_{iL}^{ab} g_{Ljck} + \sum_D \tau_{ij}^{aD} \Upsilon_{bDck} - \sum_L \tau_{iL}^{ab} \Upsilon_{Ljck} \right) \quad (13)$$

$$\tilde{\rho}_i^a += \sum_{\substack{bc \\ jk}} \tilde{R}_{ijk}^{abc} g_{jbkc} \quad (14)$$

$$\tilde{\rho}_{ij}^{ab} += \Delta_{aibj}^{-1} P_{ij}^{ab} \sum_c \left(\tilde{R}_{ijk}^{abc} F_{kc} + \tilde{\tau}_{ijk}^{abc} \Upsilon_{kc} \right) \quad (15)$$

$$\tilde{\rho}_{iL}^{ab} -= \Delta_{aibL}^{-1} P_{iL}^{ab} \left(\sum_{jk}^c \tilde{R}_{ijk}^{abc} g_{jLkc} + \sum_{jk}^{cD} \tau_{ijk}^{abc} g_{jDkc} R_L^D \right) \quad (16)$$

$$\tilde{\rho}_{ij}^{aD} += \Delta_{aiDj}^{-1} P_{ij}^{aD} \left(\sum_{bc}^k \tilde{R}_{ijk}^{abc} g_{Dbkc} - \sum_{bc}^{kL} \tilde{\tau}_{ijk}^{abc} g_{Lbkc} R_L^D \right) \quad (17)$$

The transformation of a trial vector \mathbf{L} with the transpose of the Jacobian is calculated

as follows, where σ denotes the contravariant of the transformed vector.

$$L_{ijk}^{abc} = \frac{1}{\omega - \varepsilon_{ijk}^{abc}} P_{ijk}^{abc} \left(L_i^a g_{jbkc} + L_{ij}^{ab} F_{kc} - \sum_L L_{Lk}^{ab} g_{iLjc} + \sum_D L_{jk}^{aD} g_{ibDc} \right) \quad (18)$$

$$\sigma_L^D += \sum_{\substack{abc \\ ijk}} \tilde{\tau}_{ijk}^{abc} L_{ij}^{ab} (2g_{kcLD} - 2g_{kDLc}) + \sum_{\substack{abc \\ ijk}} \tilde{\tau}_{ijk}^{abc} g_{Lbkc} L_{ij}^{aD} + \sum_{\substack{abc \\ ijk}} \tilde{\tau}_{ijk}^{abc} g_{jDkc} L_{iL}^{ab} \quad (19)$$

$$\sigma_l^D += \sum_{\substack{abcE \\ ij}} \tilde{L}_{ijl}^{abc} t_{ij}^{aE} g_{bEcD} - \sum_{\substack{abc \\ ijM}} \tilde{L}_{ijl}^{abc} t_{iM}^{ab} g_{MjcD} - \sum_{\substack{abc \\ ikM}} \tilde{L}_{ilk}^{abc} t_{iM}^{ab} g_{MDck} \quad (20)$$

$$\sigma_L^d += \sum_{\substack{ab \\ ijkM}} \tilde{L}_{ijk}^{abd} t_{iM}^{ab} g_{MjLk} - \sum_{\substack{abE \\ ijk}} \tilde{L}_{ijk}^{abd} t_{ij}^{aE} g_{LkbE} - \sum_{\substack{acE \\ ijk}} \tilde{L}_{ijk}^{adc} t_{ij}^{aE} g_{LEck} \quad (21)$$

$$\sigma_{ij}^{aD} += P_{ij}^{aD} \sum_{\substack{bc \\ k}} \tilde{L}_{ijk}^{abc} g_{bDck} \quad (22)$$

$$\sigma_{iL}^{ab} -= P_{iL}^{ab} \sum_{\substack{c \\ kl}} \tilde{L}_{ijk}^{abc} g_{Ljck} \quad (23)$$

Using Cholesky decomposition the integral g_{PQRS} are decomposed into $\sum_\chi L_{PQ}^\chi L_{RS}^\chi$ reducing the memory requirements for the integrals and intermediates.

The following equations contain the CC3 contribution to the left transition density D^{m-0}

$$D_{kl}^{m-0} -= \sum_{\substack{abc \\ ij}} \frac{1}{2} \tilde{L}_{ijl}^{abc} \tau_{ijk}^{abc} \quad (24)$$

$$D_{ld}^{m-0} += \sum_{\substack{ab \\ ij}} L_{ij}^{ab} \tilde{\tau}_{ijl}^{abd} \quad (25)$$

$$D_{LD}^{m-0} -= \sum_{\substack{abc \\ ijk}} \tilde{L}_{ijk}^{abc} \tau_{iL}^{ac} \tau_{jk}^{bD} \quad (26)$$

$$D_{cd}^{m-0} += \sum_{\substack{ab \\ ijk}} \frac{1}{2} \tilde{L}_{ijk}^{abc} \tau_{ijk}^{abd} \quad (27)$$

The ground state density D^{0-0} is obtained if \tilde{L} is substituted by $\tilde{\lambda}$.

Finally the CC3 terms for the right transition density, \tilde{D}^{0-m} .

$$\begin{aligned}
\tilde{D}_{Kl}^{0-m} &= \sum_{\substack{abc \\ ij}} \tilde{\lambda}_{ijl}^{abc} R_i^a \tau_{jK}^{bc} \\
\tilde{D}_{kl}^{0-m} &= \frac{1}{2} \sum_{\substack{abc \\ ij}} \tilde{\lambda}_{ijl}^{abc} R_{ijk}^{abc} \\
\tilde{D}_{ld}^{0-m} &= \sum_{\substack{abc \\ ijk}} \tilde{\lambda}_{ijk}^{abc} R_i^a (\tau_{jkl}^{bcd} - \tau_{jlk}^{bcd}) + \sum_{\substack{ab \\ ij}} \tilde{\lambda}_{ij}^{ab} \tilde{R}_{ijl}^{abd} \\
\tilde{D}_{LD}^{0-m} &= \frac{1}{2} \sum_{\substack{abc \\ ijk}} \tilde{\lambda}_{ijk}^{abc} R_{ij}^{ab} (2\tau_{kL}^{cD} - \tau_{Lk}^{cD}) - \sum_{\substack{abc \\ ijk}} \tilde{\lambda}_{ijk}^{abc} (R_{iL}^{ac} \tau_{jk}^{bD} + R_{ik}^{aD} \tau_{jL}^{bc}) \\
\tilde{D}_{lD}^{0-m} &= \frac{1}{2} \sum_{\substack{abc \\ ijk}} \tilde{\lambda}_{ijk}^{abc} \tau_{ijl}^{abc} R_k^D \\
\tilde{D}_{Ld}^{0-m} &= \frac{1}{2} \sum_{\substack{abc \\ ijk}} \tilde{\lambda}_{ijk}^{abc} \tau_{ijk}^{abd} R_L^c \\
\tilde{D}_{ck}^{0-m} &= \frac{1}{2} \sum_{\substack{ab \\ ij}} \tilde{\lambda}_{ijk}^{abc} R_{ij}^{ab} \\
\tilde{D}_{cD}^{0-m} &= \sum_{\substack{ab \\ ijk}} \tilde{\lambda}_{ijk}^{abc} R_i^a \tau_{jk}^{bD} \\
\tilde{D}_{cd}^{0-m} &= \sum_{\substack{ab \\ ijk}} \frac{1}{2} \tilde{\lambda}_{ijk}^{abc} R_{ijk}^{abd} \\
\tilde{D}_{LL}^{0-m} &= \frac{1}{6} \sum_{\substack{abc \\ ijk}} 2\tilde{\lambda}_{ijk}^{abc} R_{ijk}^{abc} \\
\tilde{D}_{pq}^{0-m} &= \frac{1}{6} \sum_{\substack{abc \\ ijk}} \tilde{\lambda}_{ijk}^{abc} R_{ijk}^{abc} D_{pq}^{0-0}
\end{aligned} \tag{28}$$

Guanine

Table S1 summarizes the results from calculations using MLCC3 with active spaces where $n_v = 10n_o$. These results are also visualized in Figure S1 showing a smooth convergence of both excitation energies and oscillator strengths towards the CC3 results.

Table S1: Excitation energies and oscillator strengths for the first four excited states of Guanine with MLCC3 for active spaces with increasing size. For the MLCC3 values the number of occupied and virtual orbitals is reported in the left column. The total system contains 39 occupied and 263 virtual orbitals.

System	State 1		State 2		State 3		State 4	
CCSD	535.91	3.26	538.44	0.12	539.39	0.05	539.68	0.07
8/ 80	534.13	2.45	535.20	0.06	536.22	0.10	536.34	0.00
10/100	533.94	2.39	534.99	0.06	535.79	0.11	536.08	0.00
13/130	533.79	2.30	534.78	0.06	535.43	0.13	535.77	0.01
15/150	533.73	2.26	534.66	0.06	535.18	0.14	535.64	0.01
18/180	533.66	2.21	534.55	0.05	534.94	0.14	535.44	0.01
20/200	533.62	2.18	534.49	0.05	534.83	0.16	535.32	0.01
24/240	533.55	2.14	534.41	0.05	534.69	0.17	535.14	0.02
CC3	533.51	2.12	534.36	0.05	534.59	0.15	535.01	0.02

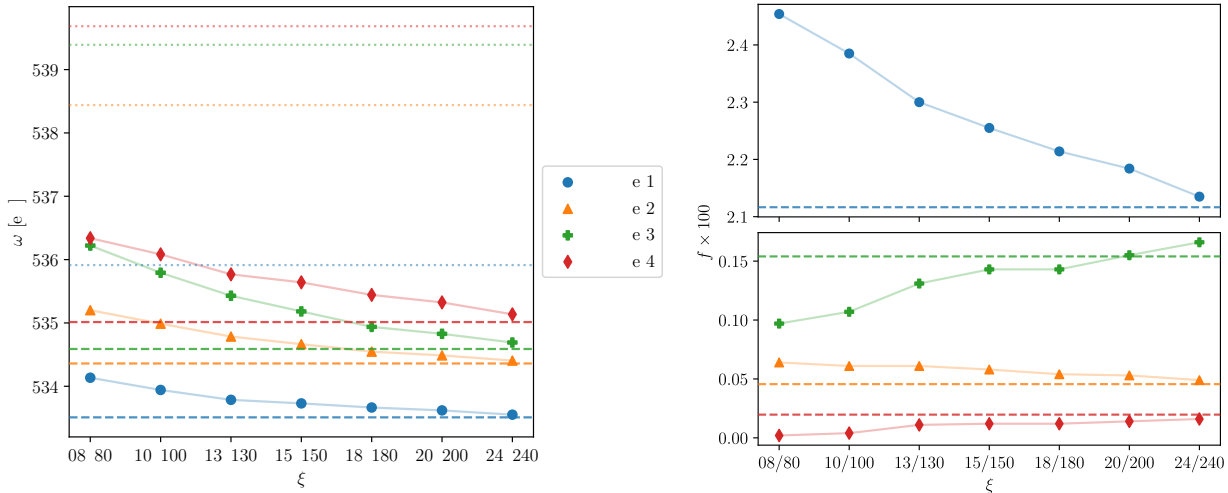


Figure S1: Convergence of the first four core excitation energies (left) and oscillator strengths (right) of guanine with the size of the active space. Dashed lines are the CC3 results and dotted lines denote the CCSD values.

Table S2: Speed up of MLCC3 compared to canonical CC3 for the calculation of four core excited states of guanine. Speed ups calculated according to equations 47 and 48 in the main document. The first part shows the speed up for terms that scale asymptotically as $\mathcal{O}(n_v n_v^3 n_o^3)$ while the second part summarizes the speed up for terms with a cost of $\mathcal{O}(n_v n_v^3 n_o^2)$.

ξ	10^{-3}	10^{-4}	10^{-5}	10^{-6}
τ	1520.1	31.2	5.9	2.3
λ	1505.2	31.6	6.0	2.5
D^{0-0}	1397.9	27.0	5.3	2.2
D^{m-0}	849.7	18.4	4.1	1.8
\tilde{D}^{0-m}	977.8	21.9	4.7	2.0
S_{theo}^{GS}	1500.2	23.4	4.9	2.3
\mathbf{R}	537.8	21.4	4.4	1.9
\mathbf{L}	502.8	20.4	4.5	2.1
S_{theo}^{ES}	615.4	15.6	3.7	1.9

Table S3: Speed up of MLCC3 compared to canonical CC3 for the calculation of a single core excited states of guanine. Speed ups calculated according to equations 47 and 48 in the main document. The first part shows the speed up for terms that scale asymptotically as $\mathcal{O}(n_v n_v^3 n_o^3)$ while the second part summarizes the speed up for terms with a cost of $\mathcal{O}(n_v n_v^3 n_o^2)$.

n_o	16	18	18	18	20	20
n_v	160	130	150	180	130	200
τ	55.4	79.1	53.9	31.6	57.9	17.7
λ	58.6	77.2	54.1	31.9	56.8	17.5
D^{0-0}	61.5	73.6	49.6	29.4	54.5	16.5
D^{m-0}	51.5	61.4	41.6	25.4	48.8	14.5
\tilde{D}^{0-m}	48.4	61.3	39.2	24.6	46.5	13.6
S_{theo}^{GS}	64.3	84.2	54.8	31.7	61.4	16.9
\mathbf{R}	23.5	34.7	24.6	14.4	28.5	9.1
\mathbf{L}	23.7	32.8	24.0	14.1	26.8	8.7
S_{theo}^{ES}	26.4	38.9	25.3	14.6	31.5	8.6

Geometries

Here we list the geometries of the molecules used in the calculations presented in the application section of the paper.

Table S4: Geometry of guanine in Ångström.

Atom	x	y	z
O	2.400 416	1.186 125	0.000 000
N	-2.164 547	0.729 374	0.000 000
C	-1.823 669	2.066 210	0.000 000
N	-0.540 931	2.253 857	0.000 000
C	0.000 000	0.987 621	0.000 000
C	1.368 570	0.557 966	0.000 000
N	1.424 157	-0.869 681	0.000 000
C	0.356 682	-1.723 002	0.000 000
N	0.627 528	-3.053 172	0.000 000
N	-0.882 076	-1.320 799	0.000 000
C	-0.996 160	0.028 079	0.000 000
H	-2.573 196	2.842 649	0.000 000
H	2.367 552	-1.232 740	0.000 000
H	1.561 780	-3.418 613	0.000 000
H	-0.152 003	-3.687 334	0.000 000
H	-3.088 910	0.328 741	0.000 000

Table S5: Geometry of formaldehyde with 6 explicit water molecules in Ångström. Adapted from a geometry with 10 water molecules from Ref. 1.

Atom	x	y	z
C	0.241 55	-0.262 33	0.506 53
O	1.088 78	-0.291 15	1.392 33
H	-0.094 79	-1.186 77	0.014 81
H	-0.218 55	0.687 84	0.177 09
O	1.675 06	2.525 13	1.365 91
H	1.641 35	1.575 95	1.596 89
H	1.726 10	2.518 33	0.384 56
O	1.750 08	-0.316 32	-1.774 58
H	1.577 21	0.658 33	-1.808 06
H	2.611 83	-0.369 28	-1.335 01
O	1.481 97	-3.011 67	1.264 13
H	2.112 76	-3.439 41	1.860 16
H	1.491 99	-2.055 96	1.511 82
O	-2.406 32	-1.194 77	0.869 90
H	-2.048 99	-2.107 72	0.678 51
H	-3.055 60	-1.308 21	1.577 78
O	-0.897 52	3.335 56	1.622 75
H	0.067 15	3.094 59	1.644 54
H	-0.910 78	4.279 66	1.838 20
O	-1.168 71	2.719 32	-1.007 01
H	-1.221 05	2.987 36	-0.053 88
H	-1.773 48	1.941 85	-1.103 82

References

- (1) Folkestad, S. D.; Koch, H. Multilevel CC2 and CCSD Methods with Correlated Natural Transition Orbitals. *J. Chem. Theory Comput.* **2020**, *16*, 179–189.